Nonrotating and rotating neutron stars in the extended field theoretical model

Shashi K. Dhiman,[1] Raj Kumar,[1] and B. K. Agrawal[2]
[1]*Department of Physics, H.P. University, Shimla 171 005, India*
[2]*Saha Institute of Nuclear Physics, Kolkata 700 064, India*
(Received 4 December 2006; revised manuscript received 25 April 2007; published 23 October 2007)

We study the properties of nonrotating and rotating neutron stars for a new set of equations of state (EOSs) with different high-density behavior obtained using the extended field theoretical model. The high-density behavior for these EOSs are varied by varying the ω-meson self-coupling and hyperon-meson couplings in such a way that the quality of fit to the bulk nuclear observables, nuclear matter incompressibility coefficient, and hyperon-nucleon potential depths remain practically unaffected. We find that the largest value for maximum mass for the nonrotating neutron star is $2.1M_{\odot}$. The radius for a neutron star with canonical mass is 12.8–14.1 km, provided only those EOSs are considered for which the maximum mass is larger than $1.6M_{\odot}$, the lower bound on the maximum mass measured so far. Our results for the very recently discovered fastest rotating neutron star indicate that this star is supramassive with mass $1.7M_{\odot}$–$2.7M_{\odot}$ and circumferential equatorial radius 12–19 km.

DOI: 10.1103/PhysRevC.76.045801 PACS number(s): 26.60.+c, 13.75.Cs, 13.75.Ev, 97.60.Jd

I. INTRODUCTION

Knowledge of neutron star properties is necessary to probe the high-density behavior of the equation of state (EOS) for baryonic matter in β equilibrium. The EOS for densities higher than $\rho_0 = 0.16$ fm^{-3} can be well constrained if radii for the neutron stars over a wide range of their masses are appropriately known. Even accurate information on the maximum neutron star mass $M_{\rm max}$ and radius $R_{1.4}$ for the neutron star with canonical mass ($1.4M_{\odot}$) would narrow down the choices for the plausible EOSs to just a few. Till date, only neutron stars with masses of around $1.4M_{\odot}$ have been accurately measured [1–3]. Recent measurement of the mass of the pulsar PSR J0751+1807 imposes lower bounds on the maximum mass of the neutron star to be $1.6M_{\odot}$ and $1.9M_{\odot}$ with 95% and 68% confidence limits, respectively [4]. The increase in the lower bounds of the neutron star maximum mass could eliminate the family of EOSs in which exotica appear and substantial softening begins (around $2\rho_0$ to $4\rho_0$), leading to appreciable reduction of the maximum mass. The available data on the neutron star radius have large uncertainties [5–9]. The main source of the uncertainties in the measurements of the neutron star radii are the unknown chemical composition of the atmosphere, inaccuracies in the star's distance, and the high magnetic field ($\sim 10^{12}$ G). The recent discovery of the binary neutron star system PSR J0737–3039A,B [2] with masses of the individual stars being $1.338M_{\odot}$ and $1.249M_{\odot}$ has raised the hope for the possibility of measuring the moment of inertia from the spin-orbit coupling effects [3]. It is expected that a reasonably accurate value for neutron star radius can be deduced from the moment of inertia measurements. The very recent discovery of the fastest rotating neutron star (with rotational frequency of 1122 Hz) observed in the X-ray transient XTE J1739–285 [10] has placed an additional constraint on the EOS at very high density [11].

Theoretically, the mass-radius relationship and compositions of neutron stars are studied by using various models, which can be broadly grouped into (i) nonrelativistic potential models [12], (ii) nonrelativistic mean-field models [13–16], (iii) field-theoretical-based relativistic mean-field (FTRMF) models [17–19], and (iv) Dirac-Brueckner-Hartree-Fock models [20–23]. Each of these models can yield EOSs with different high-density behavior, which is not yet well constrained. As a result, neutron star properties vary over a wide range even for the same model. In this work we shall mainly focus on the variations in the properties of the neutron stars obtained within the FTRMF models. The FTRMF models predict values of $M_{\rm max} = 1.2$–$3.0M_{\odot}$ and $R_{1.4} = 10$–16 km for nonrotating neutron stars [24–26]. The lower values of $M_{\rm max}$ and $R_{1.4}$ correspond to neutron stars composed of nucleons and hyperons in β equilibrium, whereas the higher values of $M_{\rm max}$ and $R_{1.4}$ correspond to neutron stars with no hyperons. We would like to emphasize that not all the different parametrizations of the FTRMF model, employed to study the neutron star properties, can reproduce satisfactorily the basic properties of finite nuclei and nuclear matter at the saturation density. For instance, the value of the nuclear matter incompressibility coefficient, which largely controls the low-density behavior of an EOS, varies between 200 and 360 MeV for different FTRMF models, although, the value of the nuclear matter incompressibility coefficient is very well constrained to 230 ± 10 MeV by experimental data on the isoscalar giant monopole resonances in heavy nuclei [27,28]. The variations in neutron star properties resulting from the differences in the high-density behavior of the different EOSs can be appropriately studied only if the low-density behavior for each of these EOSs is constrained by using the experimental data on the bulk properties of the finite nuclei and nuclear matter at the saturation density.

The extended FTRMF model [29–31] includes mixed and self-coupling terms for the σ, ω, and ρ mesons. The ω-meson self-coupling term enables one to vary the high-density behavior of the EOS without affecting nuclear matter properties at the saturation density [24]. The mixed interaction terms involving ρ mesons allow ones to significantly vary the density dependence of the symmetry energy coefficient [32–34], which plays a crucial role in determining the cooling

mechanism of a neutron star [35]. Yet, such a versatile version of the FTRMF model has not been used to fully explore variations in the properties of neutron stars resulting mainly from the uncertainties in the high-density behavior of the EOS. In the present work we use the extended FTRMF models to obtain a new set of EOSs with different high-density behavior for β-equilibrated matter composed of nucleons and hyperons. Each of these different EOSs corresponds to a different choice for the ω-meson self-coupling and hyperon-meson couplings, which mainly affects the high-density behavior of an EOS. The remaining parameters of the model are calibrated by using a set of experimental data on the total binding energy and charge rms radii for a few closed-shell nuclei. In our calibrational procedure we also use the value of neutron skin thickness for the ^{208}Pb nucleus as one of the data. Because the neutron skin thickness is only poorly known, we obtain different parameter sets for different neutron skin thickness, ranging from 0.16 to 0.28 fm. We further restrict the parameters to yield a reasonable value for the nuclear matter incompressibility coefficient at the saturation density. We use our EOSs to study the mass-radius relationship and chemical compositions for nonrotating neutron stars. For the case of rotating neutron stars, we present our results for the Keplerian sequences and also investigate the variations of mass and circumferential equatorial radius for the very recently discovered fastest rotating neutron star.

In Sec. II we outline very briefly the Lagrangian density and corresponding energy density for the extended FTRMF model. In Sec. III we present our various parametrizations for different combinations of ω-meson self-coupling, hyperon-meson couplings, and neutron skin thickness for the ^{208}Pb nucleus. In Sec. IV we present our results for nuclear matter properties at the saturation density. In this section we also discuss the quality of the fits to finite nuclei for these parametrizations. In Sec. V we present our results for the properties of nonrotating neutron stars. We also generate some rotating neutron star sequences, for which the results are presented in Sec. VI. Finally, our main conclusions are presented in Sec. VII.

II. EXTENDED FIELD THEORETICAL MODEL

The effective Lagrangian density for the FTRMF model generally describes the interactions of baryons via the exchange of σ, ω, and ρ mesons. The σ and the ω mesons are responsible for nuclear binding whereas the ρ meson is required to obtain the correct value for the empirical symmetry energy. The cubic and quartic terms for the self-interaction of the σ meson are often considered, which significantly improves the value of the nuclear matter incompressibility. Nevertheless, the values of the nuclear matter incompressibility coefficient for these models are usually larger in comparison to their values extracted from the experimental data on isoscalar giant monopole resonances. Moreover, the symmetry energy coefficient and its density dependence is also somewhat higher relative to the corresponding empirical estimates. One can easily overcome these issues in the extended FTRMF model, which includes self- and mixed interaction terms for σ, ω, and ρ mesons up to the quartic order. In particular, mixed interaction terms involving the ρ-meson field enables one to vary the density dependence of the symmetry energy coefficient and the neutron skin thickness in heavy nuclei over a wide range without affecting the other properties of finite nuclei [33,34]. The contribution from the self-interaction of ω mesons plays an important role in varying the high-density behavior of the EOS and also prevents instabilities in the calculation of the EOS [24,36]. However, the expectation value of the ρ-meson field is an order of magnitude smaller than that for the ω-meson field [31]. Thus, inclusion of the ρ-meson self-interaction can affect the properties of finite nuclei and neutron stars only very marginally [24].

The Lagrangian density for the extended FTRMF model can be written as

$$\mathcal{L} = \mathcal{L}_{BM} + \mathcal{L}_{\sigma} + \mathcal{L}_{\omega} + \mathcal{L}_{\rho} + \mathcal{L}_{\sigma\omega\rho} + \mathcal{L}_{\rm em} + \mathcal{L}_{e\mu} + L_{YY}, \tag{1}$$

where the baryonic and mesonic Lagrangian $\mathcal{L}_{BM}$ can be written as

$$\mathcal{L}_{BM} = \sum_B \overline{\Psi}_B \Big[i\gamma^\mu \partial_\mu - (M_B - g_{\sigma B}\sigma) - \left(g_{\omega B}\gamma^\mu \omega_\mu + \frac{1}{2} g_{\rho B}\gamma^\mu \tau_B . \rho_\mu \right) \Big] \Psi_B. \tag{2}$$

Here, the sum is taken over the complete baryon octet, which consists of nucleons and Λ, Σ, and Ξ hyperons. For the calculation of finite nuclei properties only the neutron and proton have been considered. τ_B are the isospin matrices. The Lagrangian describing self-interactions for σ, ω, and ρ mesons can be written as

$$\mathcal{L}_{\sigma} = \frac{1}{2}\left(\partial_\mu \sigma \partial^\mu \sigma - m_\sigma^2 \sigma^2\right) - \frac{\overline{\kappa}}{3!} g_{\sigma N}^3 \sigma^3 - \frac{\overline{\lambda}}{4!} g_{\sigma N}^4 \sigma^4, \tag{3}$$

$$\mathcal{L}_{\omega} = -\frac{1}{4}\omega_{\mu\nu}\omega^{\mu\nu} + \frac{1}{2} m_\omega^2 \omega_\mu \omega^\mu + \frac{1}{4!}\zeta g_{\omega N}^4 (\omega_\mu \omega^\mu)^2, \tag{4}$$

$$\mathcal{L}_{\rho} = -\frac{1}{4}\rho_{\mu\nu}\rho^{\mu\nu} + \frac{1}{2} m_\rho^2 \rho_\mu \rho^\mu + \frac{1}{4!}\xi g_{\rho N}^4 (\rho_\mu \rho^\mu)^2. \tag{5}$$

The field tensors $\omega^{\mu\nu}$ and $\rho^{\mu\nu}$ correspond to the ω and ρ mesons and can be defined as $\omega^{\mu\nu} = \partial^\mu \omega^\nu - \partial^\nu \omega^\mu$ and $\rho^{\mu\nu} = \partial^\mu \rho^\nu - \partial^\nu \rho^\mu$. The mixed interactions of σ, ω, and ρ mesons, $\mathcal{L}_{\sigma\omega\rho}$, can be written as

$$\mathcal{L}_{\sigma\omega\rho} = g_{\sigma N} g_{\omega N}^2 \sigma \omega_\mu \omega^\mu \left(\overline{\alpha_1} + \frac{1}{2}\overline{\alpha_1}' \sigma \right) + g_{\sigma N} g_{\rho N}^2 \sigma \rho_\mu \rho^\mu \left(\overline{\alpha_2} + \frac{1}{2}\overline{\alpha_2}' \sigma \right) + \frac{1}{2}\overline{\alpha_3}' g_{\omega N}^2 g_{\rho N}^2 \omega_\mu \omega^\mu \rho_\mu \rho^\mu. \tag{6}$$

The $\mathcal{L}_{\rm em}$ is the Lagrangian for electromagnetic interactions and can be expressed as

$$\mathcal{L}_{\rm em} = -\frac{1}{4} F_{\mu\nu} F^{\mu\nu} - \sum_B e \overline{\Psi}_B \gamma_\mu \frac{1 + \tau_{3B}}{2} A_\mu \Psi_B, \tag{7}$$

where $F^{\mu\nu} = \partial^\mu A^\nu - \partial^\nu A^\mu$. The hyperon-hyperon interaction has been included by introducing two additional mesonic fields (σ^* and ϕ) and the corresponding Lagrangian $\mathcal{L}_{YY}$

($Y = \Lambda$, Σ, and Ξ) can be written as

$$\mathcal{L}_{YY} = \sum_Y \overline{\Psi}_Y (g_{\sigma^* Y}\sigma^* - g_{\phi Y}\gamma^\mu \phi_\mu)\Psi_Y + \frac{1}{2}\left(\partial_\nu \sigma^* \partial^\nu \sigma^* - m_{\sigma^*}^2 \sigma^{*2}\right) - \frac{1}{4}S_{\mu\nu}S^{\mu\nu} + \frac{1}{2}m_\phi^2 \phi_\mu \phi^\mu. \tag{8}$$

The charge-neutral neutron star matter also includes leptons such as e^- and μ^- in addition to neutrons, proton, and hyperons at high densities. The leptonic contributions to the total Lagrangian density can be written as

$$\mathcal{L}_{e\mu} = \sum_{\ell=e,\mu} \overline{\Psi}_\ell (i\gamma^\mu \partial_\mu - M_\ell)\Psi_\ell. \tag{9}$$

The equation of motion for baryons, mesons, and photons can be derived from the Lagrangian density defined in Eq. (1). The equation of motion for baryons can be given as

$$\left[\gamma^\mu \left(i\partial_\mu - g_{\omega B}\omega_\mu - \frac{1}{2}g_{\rho B}\tau_B . \rho_\mu - e\frac{1+\tau_{3B}}{2}A_\mu - g_{\phi B}\phi^\mu\right) - (M_B + g_{\sigma B}\sigma + g_{\sigma^* B}\sigma^*)\right]\Psi_B = \epsilon_B \Psi_B. \tag{10}$$

The Euler-Lagrange equations for the ground-state expectation values of the mesons fields are

$$\left(-\Delta + m_\sigma^2\right)\sigma = \sum_B g_{\sigma B}\rho_{sB} - \frac{\overline{\kappa}}{2}g_{\sigma N}^3\sigma^2 - \frac{\overline{\lambda}}{6}g_{\sigma N}^4\sigma^3 + \overline{\alpha_1}g_{\sigma N}g_{\omega N}^2\omega^2 + \overline{\alpha_1}' g_{\sigma N}^2 g_{\omega N}^2 \sigma\omega^2 + \overline{\alpha_2}g_{\sigma N}g_{\rho B}^2\rho^2 + \overline{\alpha_2}' g_{\sigma N}^2 g_{\rho N}^2 \sigma\rho^2, \tag{11}$$

$$\left(-\Delta + m_\omega^2\right)\omega = \sum_B g_{\omega B}\rho_B - \frac{\zeta}{6}g_{\omega N}^4\omega^3 - 2\overline{\alpha_1}g_{\sigma N}g_{\omega N}^2\sigma\omega - \overline{\alpha_1}' g_{\sigma N}^2 g_{\omega N}^2 \sigma^2\omega - \overline{\alpha_3}' g_{\omega N}^2 g_{\rho N}^2 \omega\rho^2, \tag{12}$$

$$\left(-\Delta + m_\rho^2\right)\rho = \sum_B g_{\rho B}\tau_{3B}\rho_B - \frac{\xi}{6}g_{\rho N}^4\rho^3 - 2\overline{\alpha_2}g_{\sigma N}g_{\rho N}^2\sigma\rho - \overline{\alpha_2}' g_{\sigma N}^2 g_{\rho N}^2 \sigma^2\rho - \overline{\alpha_3}' g_{\omega N}^2 g_{\rho N}^2 \omega^2\rho, \tag{13}$$

$$\left(-\Delta + m_{\sigma^*}^2\right)\sigma^* = \sum_B g_{\sigma^* B}\rho_{sB}, \tag{14}$$

$$\left(-\Delta + m_\phi^2\right)\phi = \sum_B g_{\phi B}\rho_B, \tag{15}$$

$$-\Delta A_0 = e\rho_p, \tag{16}$$

where the baryon density ρ_B, scalar density ρ_{sB}, and charge density ρ_p are, respectively,

$$\rho_B = \langle \overline{\Psi}_B \gamma^0 \Psi_B \rangle = \frac{\gamma k_B^3}{6\pi^2}, \tag{17}$$

$$\rho_{sB} = \langle \overline{\Psi}_B \Psi_B \rangle = \frac{\gamma}{(2\pi)^3}\int_0^{k_B} d^3k \frac{M_B^*}{\sqrt{k^2 + M_B^{*2}}}, \tag{18}$$

$$\rho_p = \left\langle \overline{\Psi}_B \gamma^0 \frac{1+\tau_{3B}}{2}\Psi_B \right\rangle, \tag{19}$$

with γ the spin degeneracy. Here $M_B^* = M_B - g_{\sigma B}\sigma - g_{\sigma^* B}\sigma^*$ is the effective mass of the baryon species B, k_B is its Fermi momentum, and τ_{3B} denotes the isospin projections of baryon B.

The energy density of uniform matter in the extended FTRMF models is given by

$$\mathcal{E} = \sum_{j=B,\ell}\frac{1}{\pi^2}\int_0^{k_j} k^2\sqrt{k^2 + M_j^{*2}}dk + \sum_B g_{\omega B}\omega\rho_B + \sum_B g_{\rho B}\tau_{3B}\rho + \frac{1}{2}m_\sigma^2\sigma^2 + \frac{\overline{\kappa}}{6}g_{\sigma N}^3\sigma^3 + \frac{\overline{\lambda}}{24}g_{\sigma N}^4\sigma^4 - \frac{\zeta}{24}g_{\omega N}^4\omega^4 - \frac{\xi}{24}g_{\rho N}^4\rho^4 - \frac{1}{2}m_\omega^2\omega^2 - \frac{1}{2}m_\rho^2\rho^2 - \overline{\alpha_1}g_{\sigma N}g_{\omega N}^2\sigma\omega^2 - \frac{1}{2}\overline{\alpha_1}' g_{\sigma N}^2 g_{\omega N}^2 \sigma^2\omega^2 - \overline{\alpha_2}g_{\sigma N}g_{\rho N}^2\sigma\rho^2 - \frac{1}{2}\overline{\alpha_2}' g_{\sigma N}^2 g_{\rho N}^2 \sigma^2\rho^2 - \frac{1}{2}\overline{\alpha_3}' g_{\omega N}^2 g_{\rho N}^2 \omega^2\rho^2 + \frac{1}{2}m_{\sigma^*}^2\sigma^{*2} + \sum_B g_{\phi B}\phi\rho_B - \frac{1}{2}m_\phi^2\phi^2. \tag{20}$$

The pressure of uniform matter is given by

$$P = \sum_{j=B,\ell}\frac{1}{3\pi^2}\int_0^{k_j}\frac{k^4 dk}{\sqrt{k^2 + M_j^{*2}}} - \frac{1}{2}m_\sigma^2\sigma^2 - \frac{\overline{\kappa}}{6}g_{\sigma N}^3\sigma^3 - \frac{\overline{\lambda}}{24}g_{\sigma N}^4\sigma^4 + \frac{\zeta}{24}g_{\omega N}^4\omega^4 + \frac{\xi}{24}g_{\rho N}^4\rho^4 + \frac{1}{2}m_\omega^2\omega^2 + \frac{1}{2}m_\rho^2\rho^2 + \overline{\alpha_1}g_{\sigma N}g_{\omega N}^2\sigma\omega^2 + \frac{1}{2}\overline{\alpha_1}' g_{\sigma N}^2 g_{\omega N}^2 \sigma^2\omega^2 + \overline{\alpha_2}g_{\sigma N}g_{\rho N}^2\sigma\rho^2 + \frac{1}{2}\overline{\alpha_2}' g_{\sigma N}^2 g_{\rho N}^2 \sigma^2\rho^2 + \frac{1}{2}\overline{\alpha_3}' g_{\omega N}^2 g_{\rho N}^2 \omega^2\rho^2 - \frac{1}{2}m_{\sigma^*}^2\sigma^{*2} + \frac{1}{2}m_\phi^2\phi^2. \tag{21}$$

III. PARAMETERIZATIONS OF THE EXTENDED FTRMF MODEL

In this section we consider various parametrizations of the extended FTRMF model. The different parameter sets are obtained by using different values for the ω-meson self-coupling ζ, hyperon-meson couplings g_{iY} ($i = \sigma$, ω, ρ, σ^*, and ϕ mesons), and neutron skin thickness Δr for the ^{208}Pb nucleus. The parameter ζ mainly affects the high-density behavior of the EOS and cannot be well constrained by the properties of finite nuclei. The different sets of g_{iY} can be obtained to yield different EOSs for the dense matter without affecting the resulting potential depth for hyperons in nuclear matter at the saturation density. The value of Δr for a single heavy nucleus such as ^{208}Pb, which can constrain the linear density dependence of the symmetry energy, is only poorly known. The different choices for ζ, g_{iY}, and Δr are so made that they span the entire range of values as often used in the literature. We must point out that the contributions from the ρ-meson self-coupling are ignored, because their effects are found to be only marginal even for pure neutron matter at very high densities [24].

Toward our parametrizational procedure we first set hyperon-meson couplings $g_{iY} = 0$ in Eqs. (2) and (8). Then the

TABLE I. New coupling strength parameters for the Lagrangian of the extended FTRMF model as given in Eq. (1). The seven different parameter sets correspond to the different values of the neutron skin thickness Δr for the ^{208}Pb nucleus used in the fit. The value of ω-meson self-coupling ζ is equal to 0.0 for all these parametrizations. The values of Δr are in fm, the parameters $\overline{\kappa}$, $\overline{\alpha_1}$, and $\overline{\alpha_2}$ are in fm^{-1}, and m_σ values are in MeV. The masses for other mesons are taken to be $m_\omega =$ 782.5 MeV, $m_\rho = 763$ MeV, $m_\sigma^* = 975$ MeV, and $m_\phi = 1020$ MeV. For the masses of nucleons and hyperons we use $M_N =$ 939 MeV, $M_\Lambda = 1116$ MeV, $M_\Sigma = 1193$ MeV, and $M_\Xi = 1313$ MeV. The values of $\overline{\kappa}$, $\overline{\lambda}$, $\overline{\alpha_1}$, $\overline{\alpha_1}'$, $\overline{\alpha_2}$, $\overline{\alpha}_2'$, and $\overline{\alpha}_3'$ are multiplied by 10^2.

Δr	0.16	0.18	0.20	0.22	0.24	0.26	0.28
$g_{\sigma N}$	10.51369	10.65616	10.44426	10.50339	10.34061	10.48597	10.32009
$g_{\omega N}$	13.48789	13.95799	13.52239	13.80084	13.46209	13.81202	13.45113
$g_{\rho N}$	14.98497	14.32687	13.11709	12.12975	11.18278	10.39449	10.09608
$\overline{\kappa}$	2.62556	3.02154	2.43049	3.39711	3.24752	3.05611	2.82791
$\overline{\lambda}$	−0.73495	−0.45437	−0.04279	−1.15784	−1.36867	−0.86772	−1.13890
$\overline{\alpha}_1$	0.22672	0.38665	0.18121	0.44021	0.35304	0.34843	0.23357
$\overline{\alpha}_1'$	0.07325	0.07791	0.15979	0.00987	0.00725	0.052231	0.04733
$\overline{\alpha}_2$	3.05925	2.91796	2.96668	2.56759	2.27472	0.68086	0.60739
$\overline{\alpha}_2'$	1.55587	1.35016	1.25303	0.51396	0.15515	0.41389	0.33057
$\overline{\alpha}_3'$	1.50060	1.47585	0.09727	1.04562	0.52777	1.14566	0.30434
m_σ	502.23217	495.76339	497.83489	491.48257	492.76821	490.24238	491.86681

remaining coupling parameters appearing in Eqs. (2)–(6) are determined by fitting the FTRMF results to the experimental data for the total binding energies and charge rms radii for many closed-shell normal and exotic nuclei. We consider total binding energies for ^{16,24}O, ^{40,48}Ca, ^{56,78}Ni, ^{88}Sr, ^{90}Zr, ^{100,116,132}Sn, and ^{208}Pb nuclei and charge rms radii for ^{16}O, ^{40,48}Ca, ^{56}Ni, ^{88}Sr, ^{90}Zr, ^{116}Sn, and ^{208}Pb nuclei. In addition, we also fit the value of neutron skin thickness for the ^{208}Pb nucleus. Recently extracted values of neutron skin thickness for the ^{208}Pb nucleus from isospin diffusion data lie within 0.16–0.24 fm, indicating large uncertainties [37]. We generate 21 different parameter sets using different combinations of ζ and Δr. The value of ζ is taken to be 0.0, 0.03, and 0.06 and for the Δr we use 0.16, 0.18, . . . , 0.28 fm. The best-fit parameters are obtained by minimizing the χ^2 function given as

$$\chi^2 = \frac{1}{N_d - N_p} \sum_{i=1}^{N_d} \left(\frac{\mathcal{O}_i^{\rm exp} - \mathcal{O}_i^{\rm th}}{\delta_i} \right)^2, \qquad (22)$$

where N_d is the number of experimental data points and N_p the number of parameters to be fitted. The δ_i stand for theoretical errors and $\mathcal{O}_i^{\rm exp}$ and $\mathcal{O}_i^{\rm th}$ are the experimental and the corresponding theoretical values, respectively, for a given observable. Since the $\mathcal{O}_i^{\rm th}$ in Eq. (22) are calculated by using the FTRMF model, the value of χ^2 depends on the values of the parameters appearing in Eqs. (2)–(6). The theoretical errors δ_i in Eq. (22) are taken to be 1.0 MeV for the total binding energies, 0.02 fm for the charge rms radii, and 0.005 fm for the neutron skin thickness. The best-fit parameters for a given set of values of $\mathcal{O}_i^{\rm exp}$ and δ_i are searched by using the simulated annealing method [38,39]. In our earlier work [39] we have obtained parameter sets for $\zeta = 0.0$, 0.03, and 0.06 with $\Delta r = 0.18$ fm. Here too we follow the same strategy to obtain the parameter set for a given combination of Δr and ζ. In Tables I, II, and III we list the values of parameters for all the sets presently generated. We now determine the values of the hyperon-meson coupling parameters g_{iY}. These couplings can be expressed in terms of the nucleon-meson couplings using

TABLE II. Same as Table I, but with ω-meson self-coupling $\zeta = 0.03$.

Δr	0.16	0.18	0.20	0.22	0.24	0.26	0.28
$g_{\sigma N}$	10.62886	10.76147	10.73005	10.71942	10.61808	10.67656	10.60110
$g_{\omega N}$	13.65991	14.11102	14.04275	14.12534	13.88708	14.11958	14.03101
$g_{\rho N}$	14.99076	14.67414	13.69014	12.19156	10.96456	10.14811	10.00441
$\overline{\kappa}$	1.38118	1.56065	1.62316	1.61820	1.77184	1.68916	1.78793
$\overline{\lambda}$	0.58536	0.97528	0.64498	1.06102	0.48269	0.86649	0.74676
$\overline{\alpha}_1$	0.00366	0.10311	0.08281	0.10650	0.12586	0.11999	0.16088
$\overline{\alpha}_1'$	0.02717	0.05071	0.02980	0.06526	0.00052	0.04411	0.01669
$\overline{\alpha}_2$	2.89393	3.06821	3.18222	2.77747	1.18745	0.68168	0.47146
$\overline{\alpha}_2'$	1.59659	1.16255	0.47540	0.22126	1.27574	0.54787	0.52816
$\overline{\alpha}_3'$	1.52088	1.35981	0.97721	0.45581	0.28975	0.35906	0.32358
m_σ	506.50582	500.51106	499.52635	497.20745	499.12460	495.18211	494.93882

TABLE III. Same as Table I, but with ω-meson self-coupling $\zeta = 0.06$.

Δr	0.16	0.18	0.20	0.22	0.24	0.26	0.28
$g_{\sigma N}$	11.05170	11.02412	10.95765	11.01908	10.91944	11.10806	11.03151
$g_{\omega N}$	14.65579	14.66595	14.59582	14.77458	14.64700	15.19792	15.01572
$g_{\rho N}$	14.98725	14.52186	13.41111	11.94837	10.71055	10.08835	10.00666
$\overline{\kappa}$	0.66576	0.69497	0.76852	0.78002	0.90221	1.13349	0.80797
$\overline{\lambda}$	2.46427	2.44874	2.41259	2.47238	2.33265	2.51229	2.41320
$\overline{\alpha}_1$	0.00601	0.00449	0.00409	0.01469	0.03499	0.14153	0.02073
$\overline{\alpha}'_1$	0.00203	0.00526	0.01079	0.01559	0.00230	0.00085	0.01109
$\overline{\alpha}_2$	2.86236	2.58355	2.66308	2.02292	1.24695	1.18538	0.55325
$\overline{\alpha}'_2$	1.55176	1.56881	1.30876	0.90169	0.77919	0.27422	0.16326
$\overline{\alpha}'_3$	1.55307	1.58487	0.84916	0.96305	0.74863	0.40699	0.72768
m_σ	503.43838	501.37038	499.38134	497.27203	495.82388	490.83495	490.68907

the SU(6) model as

$$\begin{aligned}
\frac{1}{3}g_{\sigma N} &= \frac{1}{2}g_{\sigma\Lambda} = \frac{1}{2}g_{\sigma\Sigma} = g_{\sigma\Xi},\\
\frac{1}{3}g_{\omega N} &= \frac{1}{2}g_{\omega\Lambda} = \frac{1}{2}g_{\omega\Sigma} = g_{\omega\Xi},\\
g_{\rho N} &= g_{\rho\Sigma} = 2g_{\rho\Xi}, \quad g_{\rho\Lambda} = 0,\\
2g_{\sigma^*\Lambda} &= 2g_{\sigma^*\Sigma} = g_{\sigma^*\Xi} = \frac{2\sqrt{2}}{3}g_{\omega N}, \quad g_{\sigma^* N} = 0,\\
2g_{\phi\Lambda} &= 2g_{\phi\Sigma} = g_{\phi\Xi} = \frac{2\sqrt{2}}{3}g_{\omega N}, \quad g_{\phi N} = 0.
\end{aligned} \tag{23}$$

Neutron star properties are quite sensitive to the values of $g_{\sigma Y}$ and $g_{\omega Y}$, whereas they are not significantly affected even if the values of $g_{\sigma^* Y}$ are varied over a reasonable range for a fixed value of $g_{\Phi Y}$ [40]. For $g_{\rho Y}$, $g_{\sigma^* Y}$, and $g_{\Phi Y}$ we use the values as given by Eq. (23). The values of $g_{\sigma Y}$ and $g_{\omega Y}$ are determined by using the expressions for the hyperon-nucleon potential. The potential depth for a given hyperon species in nuclear matter at the saturation density ($\rho_{\rm sat}$) is given as

$$U_Y^{(N)}(\rho_{\rm sat}) = -g_{\sigma Y}\sigma(\rho_{\rm sat}) + g_{\omega Y}\omega(\rho_{\rm sat}). \tag{24}$$

The values of $U_Y^{(N)}$ chosen are as follows [41]:

$$\begin{aligned}
U_\Lambda^{(N)} &= -28 \text{ MeV}, \quad U_\Sigma^{(N)} = +30 \text{ MeV}, \quad \text{and}\\
U_\Xi^{(N)} &= -18 \text{ MeV}.
\end{aligned} \tag{25}$$

Normally, $g_{\sigma Y}$ is determined for a given value of $U_Y^{(N)}(\rho_{\rm sat})$ with $g_{\omega Y}$ taken from the SU(6) model. For the sake of convenience we define

$$X_{mY} = \begin{cases} \left(\frac{g_{mY}}{g_{mN}}\right) & \text{for} \quad \Lambda \text{ and } \Sigma \text{ hyperons},\\ 2\left(\frac{g_{mY}}{g_{mN}}\right) & \text{for} \quad \Xi \text{ hyperons}, \end{cases} \tag{26}$$

where m stands for σ and ω mesons. In the present work we vary $X_{\omega Y}$ from 0.5 to 0.8 [42]. In Fig. 1 we display the variations of $X_{\sigma Y}$ as a function of $X_{\omega Y}$ obtained using the parameter set corresponding to $\zeta = 0.03$ and $\Delta r = 0.22$ fm. For all other combinations of ζ and Δr the values of $X_{\sigma Y}$ are very much the same as depicted in Fig. 1. This is because properties of symmetric nuclear matter, such as binding energy per nucleon B/A, nuclear matter incompressibility coefficient K, and effective nucleon mass M_N^*, at the saturation density are very similar for all the parametrizations considered in the present work.

IV. NUCLEAR MATTER AND FINITE NUCLEI

The various properties associated with nuclear matter are obtained by using the parameter sets of Tables I, II, and III. The values of B/A, K, M_N^*, and $\rho_{\rm sat}$ for all these parameter sets lie in a narrow range. We find that $B/A = 16.11 \pm 0.04$ MeV, $K = 230.24 \pm 9.80$ MeV, $M_N^*/M_N = 0.605 \pm 0.004$, and $\rho_{\rm sat} = 0.148 \pm 0.003$ fm^{-3}. The values of the symmetry energy coefficient J and its linear density dependence,

$$L = 3\rho\frac{dJ}{d\rho}\bigg|_{\rho_{\rm sat}}, \tag{27}$$

are strongly correlated with the Δr for the ^{208}Pb nucleus used in the fit. In Fig. 2 we display the variations of J and L calculated at saturation density as a function of Δr. The values

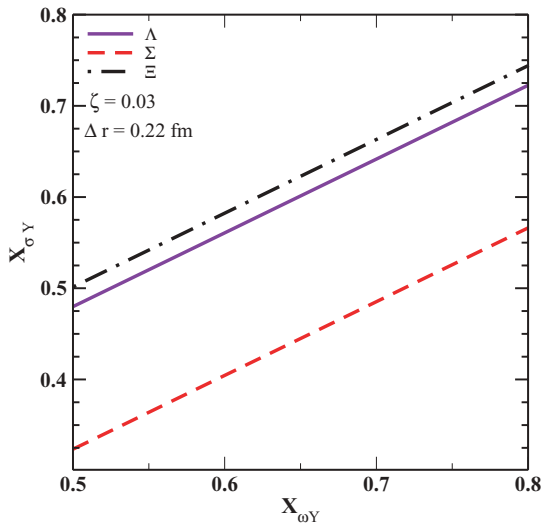

FIG. 1. (Color online) Variations of $X_{\sigma Y}$ with $X_{\omega Y}$ for Λ, Σ, and Ξ hyperons. The values of $X_{\sigma Y}$ for a given value of $X_{\omega Y}$ are calculated by using Eqs. (24) and (26).

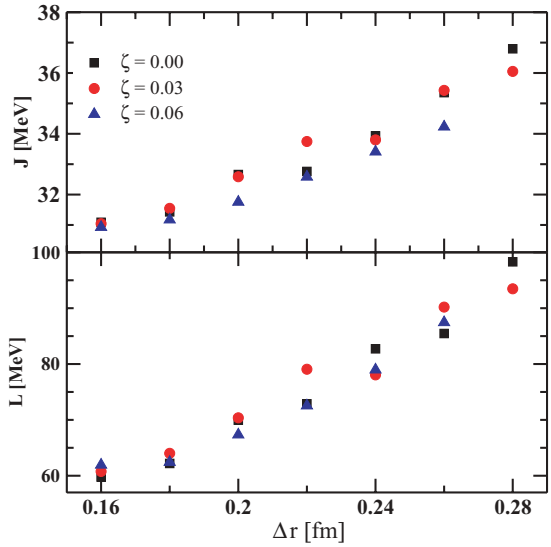

FIG. 2. (Color online) Variations of the symmetry energy coefficient J (upper panel) and its linear density dependence L (lower panel) as a function of Δr for different parametrizations with $\zeta = 0.0$, 0.03, and 0.06.

of L lie in the range 80 ± 20 MeV for Δr varying between 0.16 and 0.28 fm, which is in reasonable agreement with the recent predictions based on isospin diffusion data [37].

The relative errors in the total binding energy and charge rms radii for the nuclei included in the fits are more or less the same as we have obtained in our earlier work [39]. So, we do not wish to present here the detailed results. It might be sufficient for the present purpose to display the results for the rms errors for the total binding energies and charge rms radii obtained for our newly generated parameter sets. In Fig. 3 we plot the rms errors for the total binding energies and

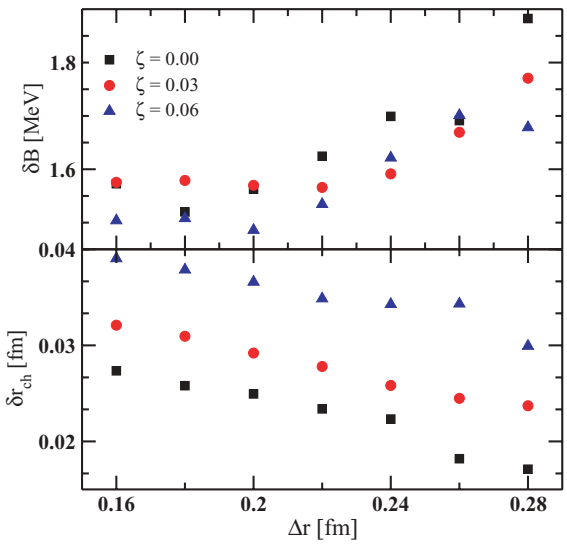

FIG. 3. (Color online) Variations of the rms errors in the total binding energies (upper panel) and charge rms radii (lower panel) as a function of Δr for different parametrizations with $\zeta = 0.0$, 0.03, and 0.06.

charge radii as a function of Δr. It is quite clear from this figure that the rms errors show hardly any variations, implying that all the parameter sets generated in the present work fit the finite nuclear properties equally well. In fact, if we do not consider the parametrizations with $\zeta = 0.0$ and $\Delta r = 0.26$ or 0.28 fm, the rms errors on the total binding energy are 1.5–1.8 MeV, which is comparable with that obtained using the NL3 parametrizations, the most commonly used [43]. The rms error of charge radii for the nuclei considered in the fit lie within the range 0.025–0.040 fm.

V. NONROTATING NEUTRON STARS

In this section we present our results for the properties of nonrotating neutron stars for a set of EOSs obtained using different parametrizations for the extended FTRMF model. Each of these parametrizations corresponds to different combinations of neutron skin thickness Δr in the ^{208}Pb nucleus, the ω-meson self-coupling ζ and hyperon-meson couplings $X_{\omega Y}$ as described in Sec. III. The values of Δr, ζ, and $X_{\omega Y}$ are so varied that they span the entire range of values often encountered in the literature. The variations in ζ and $X_{\omega Y}$ affect the high-density behavior of the EOS, whereas the density dependence of the symmetry energy coefficient is strongly correlated with Δr. It is therefore natural to expect that the variations in Δr, ζ, and $X_{\omega Y}$ can affect significantly neutron star properties. The parameters of the FTRMF model are so calibrated that the quality of fit to finite nuclei, the properties of nuclear matter at saturation density, and hyperon-nucleon potentials are almost the same for each of the parametrizations. Thus, these parametrizations provide the right starting point to study the actual variations in the properties of neutron stars resulting from the uncertainties in the EOS of dense matter.

The properties of nonrotating neutron stars are obtained by integrating the Tolman-Oppenheimer-Volkoff (TOV) equations [44]. To solve the TOV equations we use the EOS for matter consisting of nucleons, hyperons, and leptons. The composition of matter at fixed total baryon density,

$$\rho = \sum_B \rho_B, \tag{28}$$

are so determined that the charge neutrality condition

$$\sum_B q_B \rho_B + \sum_\ell q_\ell \rho_\ell = 0 \tag{29}$$

and chemical equilibrium conditions

$$\mu_B = \mu_n - q_B \mu_e, \tag{30}$$

$$\mu_\mu = \mu_e \tag{31}$$

are satisfied. In Eqs. (29)–(31) q and μ are the charge and chemical potential for various baryons and leptons considered in our calculations. For densities higher than $0.5\rho_0$, the baryonic part of the EOS is evaluated within the FTRMF model, whereas the contributions of the electrons and muons to the EOS are evaluated within the Fermi gas approximation. At densities lower than $0.5\rho_0$ down to $0.4 \times 10^{-10}\rho_0$ we use the EOS of Baym-Pethick-Sutherland (BPS) [45].

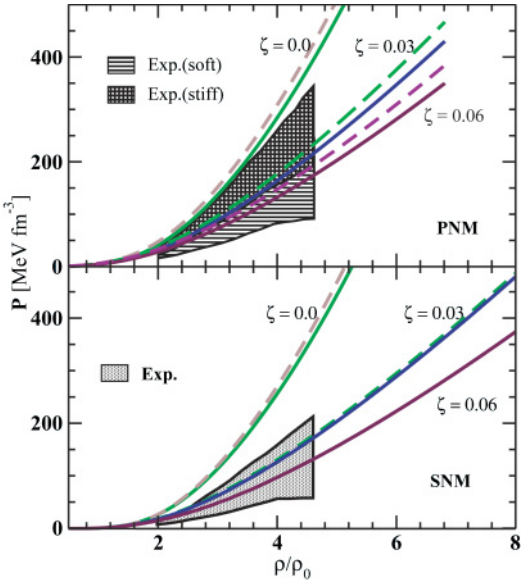

FIG. 4. (Color online) The EOSs for pure neutron matter (upper panel) and symmetric nuclear matter (lower panel). The solid and dashed curves correspond to $\Delta r = 0.16$ and 0.28 fm, respectively. The shaded regions represent the experimental data taken from Ref. [61].

In Fig. 4 we plot the EOS for pure neutron matter and symmetric nuclear matter as a function of number density for the selected combinations of ζ and Δr. We see that the EOS for $\zeta = 0.0$ is the most stiffest, and as ζ increases the EOS becomes softer. The softening of the EOS with ζ is more pronounced at higher densities. In Fig. 5 we plot our results for the neutron and electron chemical potentials as a function of baryon density obtained for the EOSs corresponding to moderate values of Δr and $X_{\omega Y}$. The chemical potentials for other particles can be evaluated by using Eqs. (30)

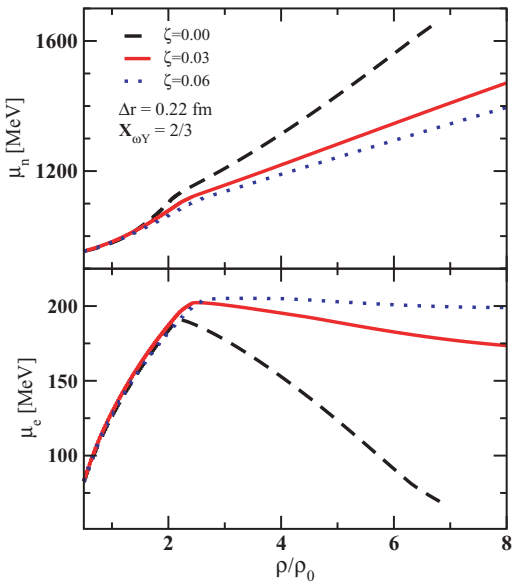

FIG. 5. (Color online) The chemical potentials for neutrons (upper panel) and electrons (lower panel) as a function of density.

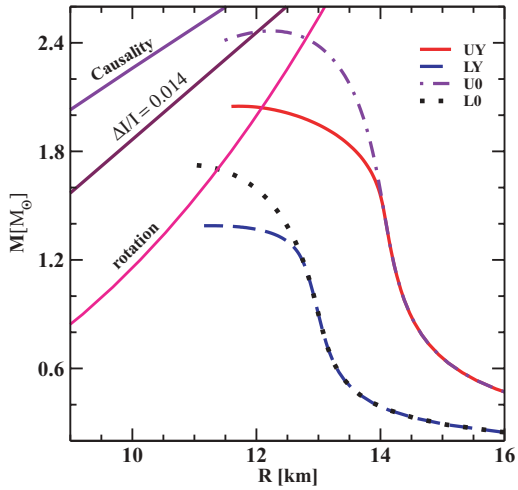

FIG. 6. (Color online) Variation of neutron star mass as a function of its radius R for selected EOSs. These EOSs are obtained by using the parameter sets LY (UY) correspond to combinations of $\Delta r = 0.16$ (0.28), $\zeta = 0.06$ (0.0), and $X_{\omega Y} = 0.5$ (0.8). The parameter sets L0 and U0 are analogous to LY and UY, respectively, but with no hyperons. The various constraints as indicated by causality, rotation, and $\Delta I/I = 0.014$ are discussed in the text.

and (31). The change in slope for neutron chemical potential versus baryon density is associated with the appearance of hyperons. The decrease in μ_e for $\rho \geqslant 2\rho_0$ is accompanied by the appearance of the Ξ^- hyperons. The maximum values of μ_e are less than half of the bare mass for kaons, which indicates that the presence of hyperons inhibits kaon condensation.

Let us now consider various neutron star properties resulting from the EOSs for the two different parameter sets (referred hereafter to as LY and UY). These parameter sets are obtained by using different combinations of $\Delta r, \zeta$, and $X_{\omega Y}$. The parameters of the LY set are obtained with $\Delta r = 0.16$ fm, $\zeta = 0.06$, and $X_{\omega Y} = 0.5$, and the UY parametrization is obtained with $\Delta r = 0.28$ fm, $\zeta = 0.0$, and $X_{\omega Y} = 0.8$. Among all the parametrizations as obtained in Sec. III, LY and UY yield the softest and the stiffest EOSs, respectively. Thus, maximum variations in neutron star properties can be studied by using the EOSs obtained for the LY and UY parameter sets. For the comparison, we also present our results for the L0 and U0 parameter sets, which are similar to the LY and UY parametrizations, but, without the hyperons. In Fig. 6 we present our results for the mass-radius relationship for LY, UY, L0, and U0 parametrizations. The region bounded by $R \leqslant 3GM/c^2$ is excluded by the causality limit [46]. The line labeled $\Delta I/I = 0.014$ is the radius limit estimated by Vela pulsar glitches [47]. The rotation constraint as indicated in Fig. 6 is obtained from [48]

$$\nu_k = 1833\eta \left(\frac{M}{M_\odot}\right)^{1/2} \left(\frac{10\ \text{km}}{R}\right)^{3/2} \text{Hz}, \qquad (32)$$

with $\eta = 0.57$ and $\nu_k = 1122$ Hz, which corresponds to the frequency for the fastest rotating neutron star present in the recently observed X-ray transient XTE J1739–285 [10]. The renormalization factor η accounts for the effects of deformation and gravity. We also calculate the variations in

TABLE IV. The values of central baryon density ρ_c, mass M, radius R, radiation radius R_∞, binding energy $E_{\rm bind}$, and redshift Z for nonrotating neutron stars with maximum mass calculated for the EOSs obtained by using LY, UY, L0, and U0 parametrizations. The parameter sets LY (L0) and UY (U0) yield the softest and stiffest EOS with (without) hyperons in comparison to all other parametrizations obtained in Sec. III.

	LY	UY	L0	U0
ρ_c (fm^{-3})	1.05	0.84	1.12	0.79
M ($M_\odot$)	1.4	2.1	1.7	2.4
R (km)	11.3	12.0	10.9	12.2
R_∞ (km)	14.2	17.3	14.9	18.9
$E_{\rm bind}$ (10^{53} ergs)	1.36	3.80	2.76	6.49
Z	0.25	0.41	0.37	0.57

the radiation radius,

$$R_\infty = \frac{R}{\sqrt{1-\frac{2GM}{Rc^2}}}, \tag{33}$$

for a neutron star with the canonical mass $1.4M_\odot$. It can be verified by using the results for the LY and UY cases presented in Fig. 6 that R_∞ lies in the range 14.2–16.8 km. Similarly, without the inclusion of hyperons, the values of R_∞ vary in the range 15.3–16.8 km. In Tables IV and V we collect a few important bulk properties for nonrotating neutron stars with maximum and canonical masses. We see that the values of $M_{\rm max}$ with the inclusion of hyperons vary between $1.4M_\odot$ and $2.1M_\odot$. Once the contributions from the hyperons are ignored $M_{\rm max}$ varies between $1.7M_\odot$ and $2.4M_\odot$. The values of $R_{1.4}$ vary from 11.3 to 14.1 km and from 12.5 to 14.1 km depending on whether the hyperonic contributions are included or not. Thus, combining our results for neutron stars with and without hyperons we find that the values of $M_{\rm max}$ and $R_{1.4}$ obtained within the FTRMF model can vary by about $1M_\odot$ and 3 km, respectively. These variations are almost half of those obtained earlier by using the FTRMF model in which bulk nuclear observables and nuclear matter incompressibility were not fitted appropriately. The values of redshift given in Tables IV and V are obtained for the ratio M/R as

$$Z = \frac{1}{\sqrt{1-\frac{2GM}{Rc^2}}} - 1. \tag{34}$$

TABLE V. Same as Table IV, but for the nonrotating neutron stars with canonical mass.

	LY	UY	L0	U0
ρ_c (fm^{-3})	1.05	0.32	0.50	0.32
R (km)	11.3	14.1	12.5	14.1
R_∞ (km)	14.2	16.8	15.3	16.8
$E_{\rm bind}$ (10^{53} ergs)	1.36	1.10	1.37	1.10
Z	0.25	0.19	0.22	0.19

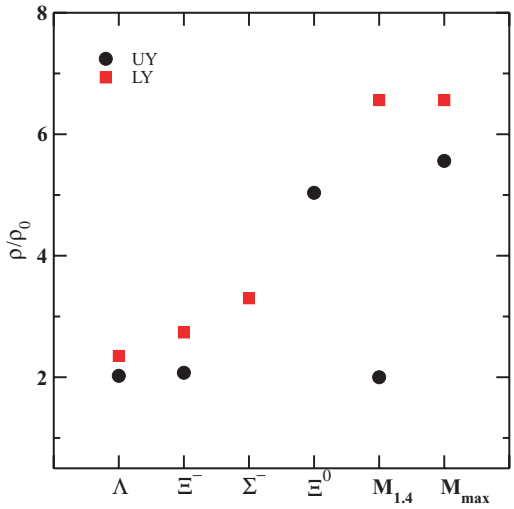

FIG. 7. (Color online) The threshold density for various hyperons and central densities for a neutron star with the canonical mass and maximum mass obtained for the EOSs corresponding to the parameter sets LY and UY.

Our results for the values of redshift for a neutron star with canonical mass are 0.22 ± 0.03. It is also interesting to note that $Z \geqslant 0.35$ only for stars with masses $1.7M_\odot$ or larger.

In Fig. 7 we have plotted the threshold densities for various hyperon species. In the same figure we also show the values of central densities for neutron stars with canonical mass and maximum mass. The threshold density is lowest for the Λ hyperons. It is interesting to note that for the UY case the threshold density for the Λ hyperons is almost equal to the central density for th neutron star with the canonical mass. This implies that the properties of the neutron star with the canonical mass do not get affected by the hyperons for the UY parametrization. This is the reason why our results for the mass and radius for U0 and UY parametrizations are very similar for neutron stars with masses up to $1.6M_\odot$, as can be seen from Fig. 6. The Σ^+ and Σ^0 hyperons do not appear in the density range relevant for the present study. However, for the TM1 parametrization of the FTRMF model one finds that all kinds of hyperons appear well below $7\rho_0$ [49,50]. This seems to be due to the large value of the nuclear matter incompressibility coefficient ($K = 281$ MeV) associated with the TM1 parameter set. In other words, not only do the variations in the properties of the neutron stars get reduced but the chemical compositions for these stars can also become different if the parameters of the FTRMF models are calibrated appropriately. In Fig. 8 we plot the particle fractions as a function of radial coordinate. These fractions are calculated for neutron stars with $M_{\rm max} = 1.4M_\odot$ and $2.1M_\odot$, corresponding to the LY (upper panel) and UY (lower panel) parametrizations, respectively. The neutron fractions in Fig. 8 are plotted after dividing them by a factor of 3. We see that the compositions of the neutron stars shown in the upper and lower panels are not the same. For the case of LY parametrizations, Ξ^- and Σ^- hyperons appear more or less simultaneously. For the UY case, Ξ^0 hyperons appear instead of Σ^- hyperons. It is noteworthy that for the case with UY parametrization the hyperons are the

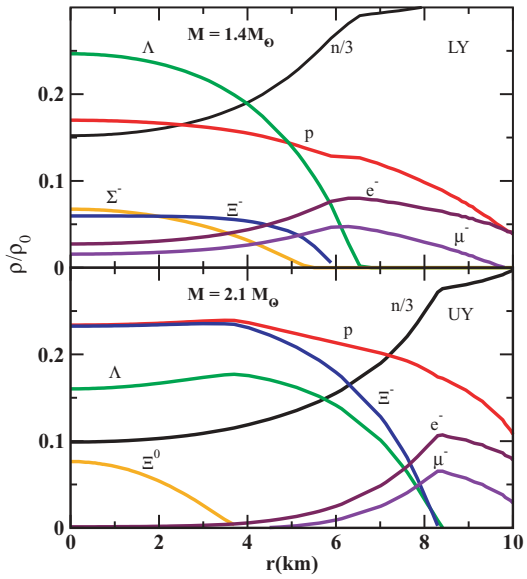

FIG. 8. (Color online) Particle fractions as a function of radial coordinate of the neutron star obtained at maximum mass for LY (upper panel) and UY (lower panel) parametrizations. The curves labeled as "n/3" should be multiplied by 3 to get the actual neutron fractions.

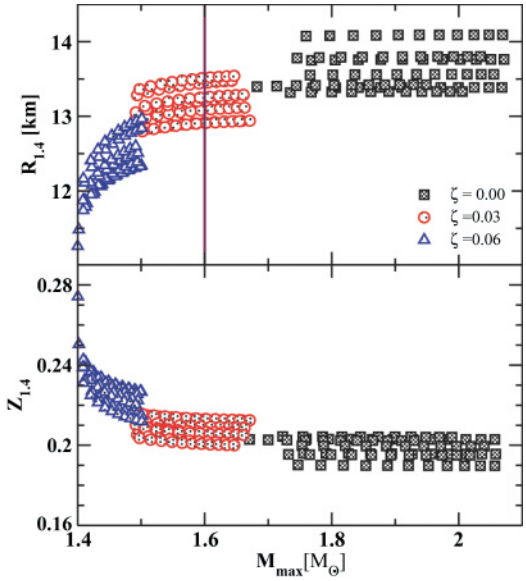

FIG. 9. (Color online) Variations of radius ($R_{1.4}$) and redshift ($Z_{1.4}$) for a neutron star with the canonical mass as a function of maximum neutron star mass obtained for the EOSs corresponding to the all different parametrizations of the extended FTRMF model as considered. The vertical line at $M_{\rm max} = 1.6M_\odot$ in the upper panel corresponds to the mass of the PSR J0751+1807 measured with a 95% confidence limit.

dominant particles at the interior ($r < 4$ km) of the neutron star, leading to complete deleptonization. We see from Fig. 8 that the proton fractions for both cases are greater than the critical value (∼15%) for the direct Urca process to occur [35].

We now consider our results for neutron star properties at the canonical and maximum masses for the set of EOSs obtained by using all the different parametrizations as given in Sec. III. These different parametrizations correspond to different combinations of $\Delta r, \zeta$, and $X_{\omega Y}$. The values of $\Delta r, \zeta$, and $X_{\omega Y}$ vary in the ranges 0.16–0.28 fm, 0.0–0.06, and 0.5–0.8, respectively. Knowledge of $M_{\rm max}$ and ($R_{1.4}$) or moment of inertia ($\mathcal{I}_{1.4}$) for neutron stars with canonical mass are very important for understanding the behavior of the EOS over the wide range of density well above ρ_0. The discovery of the pulsars PSR J0737–3039A,B and PSR J0751+1807 have raised hope for the availability of more accurate information about these quantities in the near future. The maximum mass $M_{\rm max}$ probes the densest segment of the EOS, whereas $R_{1.4}$ or $\mathcal{I}_{1.4}$ probe the relatively lower density region of the EOS. It is not possible to say a priori whether or not $M_{\rm max}$ is correlated with the properties of a neutron star with mass $1.4M_\odot$. Earlier studies using FTRMF models indicate some correlations between $M_{\rm max}$ and $R_{1.4}$ [19]. Another study carried out for 25 EOSs taken from different models show hardly any correlations between $M_{\rm max}$ and $\mathcal{I}_{1.34}$ [51]. In Fig. 9 we plot the variations of radius and the redshift for a neutron star with the canonical mass as a function of $M_{\rm max}$. We see that $M_{\rm max}$ varies between $1.4M_\odot$ and $2.1M_\odot$ and $R_{1.4}$ varies between 11.3 and 14.1 km. The vertical line at $M_{\rm max} = 1.6M_\odot$ corresponds to the mass of the PSR J0751+1807 measured with a 95% confidence limit. If only those EOSs for which $M_{\rm max} \geqslant 1.6M_\odot$ are considered then the value of $R_{1.4}$ would lie in the range 12.8–14.1 km. This result is in reasonable agreement with $R_{1.4} = 14.8^{+1.8}_{-1.6}$ km, as deduced very recently by adequately fitting the high-quality X-ray spectrum from the neutron star X7 in the globular cluster 47 Tucanae [52]. We also note strong correlations of $M_{\rm max}$ with $R_{1.4}$ and $Z_{1.4}$. For a given value of $M_{\rm max}$, the spread in the values of $R_{1.4}$ is 0.7 ± 0.1 km. Only for $M_{\rm max} \sim 1.4M_\odot$ do we find that the spread in the values of $R_{1.4}$ is ~ 0.3 km. To understand this better, we list in Table VI the values of $M_{\rm max}$ and $R_{1.4}$ obtained for the sets of EOSs corresponding to the selected combinations of Δr, ζ, and $X_{\omega Y}$. For additional information we also give in Table VI the values of $R_{\rm max}$ that correspond to the radius of a neutron star with maximum mass. It is clear from the table that for smaller ζ the value of $R_{1.4}$ varies with Δr and is independent of $X_{\omega Y}$. This is because, for smaller ζ, the central density for a neutron star with mass $1.4M_\odot$ is lower or almost equal to the threshold density for hyperons (see also Fig. 7). As ζ increases, the central density becomes larger than the threshold densities for various hyperons, and thus $R_{1.4}$ depends on Δr as well as $X_{\omega Y}$. In Fig. 10 we plot the variations of $R_{\rm max}$ and $Z_{\rm max}$ versus the maximum neutron star mass. We see that the correlations in the values of $M_{\rm max}$ and $R_{\rm max}$ are stronger than the ones observed in the case of $M_{\rm max}$ and $R_{1.4}$. The spread in the values of $R_{\rm max}$ is only 0.2 ± 0.1 km for a fixed value of $M_{\rm max}$. The values of $R_{\rm max}$ do not depend strongly on the choice of Δr, as can be seen from Table VI. The horizontal line in the lower panel corresponds to the measured value of the redshift, $Z = 0.35$, for the neutron star EXO 0748–676 [53]. For $Z = 0.35$, we find that $M_{\rm max} \sim 1.8M_\odot$ and the corresponding radius is ∼12 km. These values for neutron star masses and the corresponding radii are in reasonable agreement with the best suggested values of the

TABLE VI. Values of the M_{max}, $R_{1.4}$, and the radius R_{max} for a neutron star with maximum mass obtained for the EOSs corresponding to the selected combinations of Δr, ζ, and $X_{\omega Y}$.

		$\zeta = 0.0$			$\zeta = 0.06$		
$X_{\omega Y}$	Δr (fm)	M_{max} ($M_\odot$)	$R_{1.4}$ (km)	R_{max} (km)	M_{max} ($M_\odot$)	$R_{1.4}$ (km)	R_{max} (km)
0.50	0.16	1.8	13.4	12.0	1.4	11.3	11.3
	0.28	1.8	14.1	12.2	1.4	11.6	11.6
0.80	0.16	2.1	13.4	12.0	1.5	12.3	11.0
	0.28	2.1	14.1	12.1	1.5	13.0	11.3

mass, $1.8M_\odot$, and radius, 11.5 km, corresponding to $Z = 0.35$ [54].

To this end, we would like to mention that the calculations are repeated for an attractive Σ-N potentials by assuming $U_\Sigma^{(N)} = -30$ MeV in Eq. (24). We find that with this choice of $U_\Sigma^{(N)}$ our results for the variations in M_{max} and $R_{1.4}$ do not get affected. However, the threshold density for the Σ^- hyperon becomes lowest and the Ξ^- hyperon does not appear even for the maximum neutron star mass. It must be pointed out that the tensor coupling of the ω meson to the hyperons, not considered in the present work, could increase the value of M_{max} by about $0.1M_\odot$ [55]. We also remark that the effects of the exchange and of the correlations are not considered explicitly but are taken into account at least partly through the nonlinear self- and mixed interactions of the mesons [29,30]. Equations (11)–(16) can be interpreted as the Khon-Sham equations in the relativistic case and in this sense they include effects beyond the Hartree approach through the nonlinear couplings. However, a more accurate treatment of the exchange and correlation effects should be pursued [56,57].

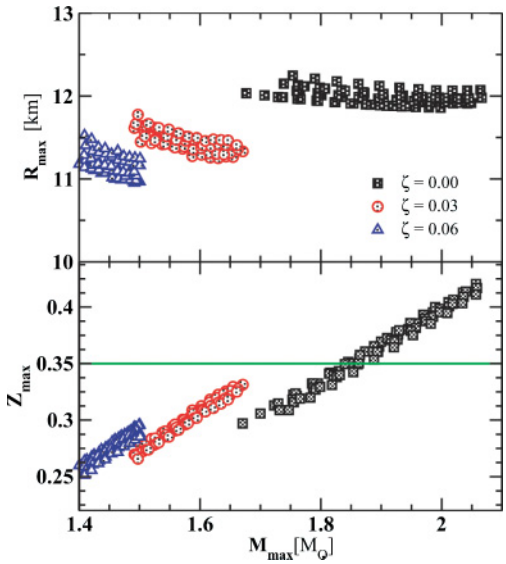

FIG. 10. (Color online) Variations of radius (R_{max}) and redshift (Z_{max}) for a neutron star with the maximum mass as a function of maximum neutron star mass obtained for the EOSs corresponding to the all different parametrizations of the extended FTRMF model as considered. The horizontal line in the lower panel corresponds to the measured value of the redshift, $Z = 0.35$, for the neutron star EXO 0748–676 [53].

VI. ROTATING NEUTRON STARS

The properties of neutron stars can get significantly affected in the presence of rotation. The effects of rotation on neutron star properties are pronounced when the frequency of rotation is close to its Keplerian limit. Earlier studies indicate that the Keplerian frequency is ~1000 Hz for neutron stars with mass around $1M_\odot$ [58]. Only very recently [10] has a neutron star rotating at 1122 Hz been discovered in the X-ray transient XTE J1739–285. In this section we shall discuss our results for the rotating neutron stars obtained by using the extended FTRMF model. These results are obtained by solving the Einstein equations for stationary axisymmetric space-time. The numerical computations are performed by using the code written by Stergioulas [59].

In Fig. 11 we plot neutron star mass versus circumferential equatorial radius R_{eq} for the Keplerian sequences obtained by using EOSs for the LY, UY, L0, and U0 parametrizations of our model. The maximum mass of the neutron stars varies between $1.7M_\odot$ and $2.5M_\odot$ and between $2.0M_\odot$ and $3.0M_\odot$ for the

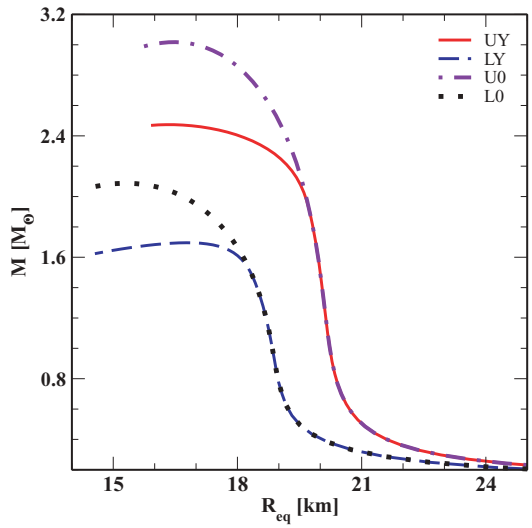

FIG. 11. (Color online) The relationship between mass M and the circumferential equatorial radius R_{eq} for Keplerian sequences for different EOSs obtained within the extended FTRMF model.

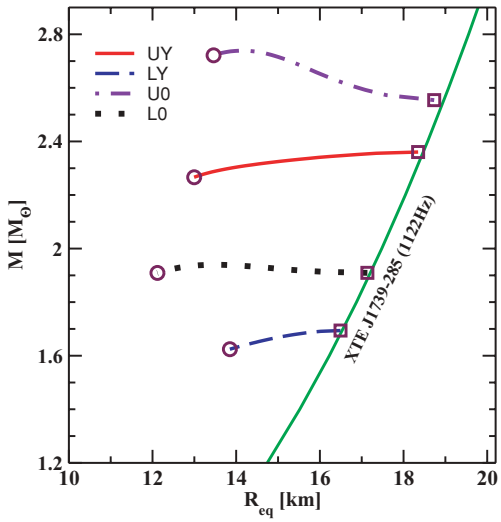

FIG. 12. (Color online) The mass M verses the circumferential equatorial radius R_{eq} for neutron stars rotating at 1122 Hz for selected EOSs obtained within the extended FTRMF model. The minimum values for the radius indicated by open circles are determined by the setting-in of the instability with respect to axisymmetric perturbations. The maximum values for the radius indicated by open squares are determined by the mass-shedding instability. The values of maximum radius are well fitted by the solid curve obtained using Eq. (35).

cases with and without hyperons, respectively. The values of $R_{eq}^{1.4}$ lie in the range 18.4–20.0 km irrespective of whether or not hyperonic degrees of freedom are included, because the central density for the canonical mass in the presence of rotation becomes lower than the threshold densities for the hyperons. The Keplerian frequencies at maximum neutron star mass for the various cases shown in Fig. 11 lie in the range 1320–1560 Hz. This means that all the EOSs obtained in the present work can yield neutron stars rotating at 1122 Hz. In Fig. 12 we plot the mass and the corresponding values for R_{eq} for a neutron star rotating at 1122 Hz. The lower and upper bounds on the radii R_{eq} are determined by the setting-in of the axisymmetric perturbation and mass-shedding instabilities, respectively [60]. The maximum values of R_{eq} are well fitted by [60]

$$R_{eq}^{max} = 13.87 \left(\frac{M}{M_\odot}\right)^{1/3} \text{ km}, \tag{35}$$

which can be obtained by using $\nu_k = 1122$ Hz and $\eta = 1$ in Eq. (32). In Table VII, we give the minimum and maximum values for R_{eq} and the corresponding neutron star mass for the various cases plotted in Fig. 12. We get $R_{eq}^{min} = 12.1$–13.8 km and $R_{eq}^{max} = 16.5$–18.7 km. The values of $M(R_{eq}^{min})$ and $M(R_{eq}^{max})$ are in the ranges 1.6–2.7$M_\odot$ and 1.7–2.6$M_\odot$, respectively. The absolute difference between $M(R_{eq}^{min})$ and $M(R_{eq}^{max})$, which gives the variations in the neutron star mass for a given EOS, is at most 0.2$M_\odot$. We also find that the baryonic masses for the neutron stars rotating with 1122 Hz for all the cases considered here are larger than the maximum baryonic mass for the corresponding nonrotating sequences. This suggests that the recently discovered fastest rotating neutron star rotating with 1122 Hz is supramassive. We also list in Table VII the values for the flattening parameter (r_{pole}/r_{eq}) and $T/|W|$, where T is the kinetic energy and W is the gravitational energy.

TABLE VII. The properties of a neutron star rotating with 1122 Hz for different EOSs calculated within the FTRMF model.

EOS	$M(R_{eq}^{min})$ ($M\odot$)	R_{eq}^{min} (km)	r_{pole}/r_{eq}	$T/\|W\|$
L0	1.908	12.12	0.804	0.054
U0	2.721	13.46	0.815	0.063
LY	1.624	13.85	0.692	0.076
UY	2.266	12.99	0.799	0.059
EOS	$M(R_{eq}^{max})$ ($M\odot$)	R_{eq}^{max} (km)	r_{pole}/r_{eq}	$T/\|W\|$
L0	1.909	17.14	0.566	0.109
U0	2.556	18.73	0.556	0.127
LY	1.694	16.49	0.575	0.097
UY	2.360	18.35	0.559	0.118

VII. CONCLUSIONS

We have used the extended FTRMF model to obtain a new set of EOSs with different high-density behavior. These EOSs are then employed to study the variations in the properties of nonrotating and rotating neutron stars. The high-density behavior of the EOS, which is not yet well constrained, is varied by choosing different values of the ω-meson self-coupling and the couplings of the ω meson to the various hyperons in our model. The different values for these couplings are so chosen that they span the entire range often considered in earlier works. The remaining parameters of the models are calibrated to yield a reasonable fit to the bulk nuclear observables, nuclear matter incompressibility coefficient, and hyperon-nucleon potential depths. The properties of finite nuclei and nuclear matter associated with each of the parametrizations used for obtaining these EOSs can be summarized as follows. The rms errors for the total binding energies and charge radii calculated for the nuclei considered in the fits are 1.5–1.8 MeV and 0.025–0.040 fm. The binding energy per nucleon is 16.11 ± 0.04 MeV, the saturation density is 0.148 ± 0.003 fm^{-3}, and the nuclear matter incompressibility coefficient is 230.24 ± 9.80 MeV.

Values of M_{max} for nonrotating neutron stars composed of nucleons and hyperons in β equilibrium can vary between 1.4$M_\odot$ and 2.1$M_\odot$. The radius $R_{1.4}$ for such neutron stars can vary in the range 11.3–14.1 km. The values of $R_{1.4}$ narrow down to only 12.8–14.1 km if one considers the EOSs for which M_{max} is larger than 1.6$M_\odot$ (which is the highest mass measured for PSR J0751+1807 with a 95% confidence limit). This result is in reasonable agreement with $R_{1.4} = 14.8^{+1.8}_{-1.6}$ km, as deduced very recently by adequately fitting the high-quality X-ray spectrum from the neutron star X7 in the globular cluster 47 Tucanae [52]. We also note strong correlations between the values of M_{max} and $R_{1.4}$.

The values of the redshift for neutron stars with canonical and maximum masses are also calculated. The redshift for a neutron star with canonical mass obtained for different EOSs varies between 0.19 and 0.25. The maximum value for the redshift is 0.41, which corresponds to the maximum neutron star mass of $2.1M_{\odot}$. For the measured value of redshift equal to 0.35, we find that the neutron star mass is $\sim 1.8M_{\odot}$ and the corresponding radius is $\sim$12 km. These values for neutron star masses and the corresponding radii are in reasonable agreement with the best suggested values of the mass, $1.8M_{\odot}$, and radius, 11.5 km, for $Z = 0.35$ [54]. For the sake of comparison we have presented our results obtained without the inclusion of the hyperons. In this case the $M_{\max}$ and $R_{1.4}$ lie in the ranges 1.7–$2.4M_{\odot}$ and 12.5–14.1 km, respectively.

We use our EOSs to compute the properties of rotating neutron stars. In particular, we studied the mass and the circumferential equatorial radius for a neutron star rotating at 1122 Hz as recently observed [10]. Our results for different EOSs indicate that the mass for such a star can lie within 1.6–$2.7M_{\odot}$. The minimum values for the circumferential equatorial radius determined by the onset of the instability with respect to the axisymmetric perturbation are found to vary in the range 12.1–13.8 km. The maximum values for the circumferential equatorial radius obtained by the mass-shedding limit vary within 16.5–18.7 km. Looking into the results for the baryonic mass we find that a neutron star rotating at 1122 Hz is supramassive for our EOSs.

ACKNOWLEDGMENTS

We would like to thank D. Bandyopadhyay for useful discussions. This work was supported in part by the University Grant Commission under Grant No. F.17-40/98 (SA-I). Shashi K. Dhiman and Raj Kumar greatly acknowledge the financial support from the Saha Institute of Nuclear Physics, Kolkata, India.

[1] S. E. Thorsett and D. Chakrabarty, Astrophys. J. **512**, 288 (1999).
[2] M. Burgay, N. D'Amico, A. Possenti, R. N. Manchester, A. G. Lyne, B. C. Joshi, M. A. McLaughlin, F. C. M. Kramer, J. M. Sarkissian, V. Kalogera, C. Kim *et al*., Nature (London) **426**, 531 (2003).
[3] A. Lyne *et al*., Science **303**, 1153 (2004).
[4] D. J. Nice, E. Splaver, I. Stairs, O. Lohmer, A. J. A. Jessner, M. Kramer, and J. Cordes, Astrophys. J. **634**, 1242 (2005).
[5] R. Rutledge, L. Bildsten, E. Brown, G. Pavlov, and V. Zavlin, Astrophys. J. **578**, 405 (2002).
[6] R. Rutledge, L. Bildsten, E. Brown, G. Pavlov, and V. Zavlin, Astrophys. J. **577**, 346 (2002).
[7] B. Gendre, D. Barret, and N. A. Webb, Astron. Astrophys. **400**, 521 (2003).
[8] W. Becker and *et al*., Astrophys. J. **594**, 364 (2003).
[9] J. Cottam, F. Paerels, and M. Mendez, Nature (London) **420**, 51 (2002).
[10] P. Kaaret, Z. Prieskorn, J. in 't Zand, S. Brandt, N. Lund, S. Mereghetti, D. Gotz, E. Kuulkers, and J. Tomsick, Astrophys. J. **657**, L97 (2006).
[11] G. Lavagetto, I. Bombaci, A. D'Ai', I. Vidana, and N. Robba, astro-ph/0612061.
[12] V. R. Pandharipande and R. A. Smith, Nucl. Phys. **A237**, 507 (1975).
[13] E. Chabanat, P. Bonche, P. Haensel, J. Meyer, and R. Schaeffer, Nucl. Phys. **A627**, 710 (1997).
[14] J. R. Stone, J. C. Miller, R. Koncewicz, P. D. Stevenson, and M. R. Strayer, Phys. Rev. C **68**, 034324 (2003).
[15] L. Monras, Eur. Phys. J. A **24**, 293 (2005).
[16] B. K. Agrawal, S. K. Dhiman, and R. Kumar, Phys. Rev. C **73**, 034319 (2006).
[17] M. Prakash, J. R. Cooke, and J. M. Lattimer, Phys. Rev. D **52**, 661 (1995).
[18] N. K. Glendenning and J. Schaffner-Bielich, Phys. Rev. C **60**, 025803 (1999).
[19] A. W. Steiner, M. Prakash, J. M. Lattimer, and P. Ellis, Phys. Rep. **411**, 325 (2005).
[20] H. Müther, M. Prakash, and T. L. Ainsworth, Phys. Lett. **B199**, 469 (1987).
[21] L. Engvik, M. Hjorth-Jensen, E. Osnes, G. Bao, and E. Østgaard, Phys. Rev. Lett. **73**, 2650 (1994).
[22] L. Engvik, E. Osnes, M. Hjorth-Jensen, G. Bao, and E. Østgaard, Astrophys. J. **469**, 794 (1996).
[23] H. J. Schulze, A. Polls, A. Ramos, and I. Vidana, Phys. Rev. C **73**, 058801 (2006).
[24] H. Müller and B. D. Serot, Nucl. Phys. **A606**, 508 (1996).
[25] A. R. Taurines, C. A. Z. Vasconcellos, M. Malherio, and M. Chiapparini, Phys. Rev. C **63**, 065801 (2001).
[26] T. K. Jha, P. K. Raina, P. K. Panda, and S. K. Patra, Phys. Rev. C **74**, 055803 (2006); [Erratum-*ibid*. **75**, 029903 (2007)].
[27] P. G. Reinhard, Nucl. Phys. **A649**, 305c (1999).
[28] D. H. Youngblood, Y.-W. Lui, and H. L. Clark, Phys. Rev. C **65**, 034302 (2002).
[29] R. Furnstahl, B. D. Serot, and H.-B. Tang, Nucl. Phys. **A598**, 539 (1996).
[30] R. Furnstahl, B. D. Serot, and H.-B. Tang, Nucl. Phys. **A615**, 441 (1997).
[31] B. D. Serot and J. D. Walecka, Int. J. Mod. Phys. E **6**, 515 (1997).
[32] C. J. Horowitz and J. Piekarewicz, Phys. Rev. Lett. **86**, 5647 (2001).
[33] R. Furnstahl, Nucl. Phys. **A706**, 85 (2002).
[34] T. Sil, M. Centelles, X. Vinas, and J. Piekarewicz, Phys. Rev. C **71**, 045502 (2005).
[35] J. M. Lattimer, C. J. Pethick, M. Prakash, and P. Haensel, Phys. Rev. Lett. **66**, 2701 (1991).
[36] Y. Sugahara and H. Toki, Nucl. Phys. **A579**, 557 (1994).
[37] L.-W. Chen, C. M. Ko, and B.-A. Li, Phys. Rev. C **72**, 064309 (2005).
[38] B. K. Agrawal, S. Shlomo, and V. K. Au, Phys. Rev. C **72**, 014310 (2005).
[39] R. Kumar, B. K. Agrawal, and S. K. Dhiman, Phys. Rev. C **74**, 034323 (2006).
[40] I. Bednarek and R. Manka, J. Phys. G **31**, 1009 (2005).
[41] J. Schaffner-Bielich and A. Gal, Phys. Rev. C **62**, 034311 (2000).
[42] N. K. Glendenning and S. A. Moszkowski, Phys. Rev. Lett. **67**, 2414 (1991).
[43] G. A. Lalazissis, J. Konig, and P. Ring, Phys. Rev. C **55**, 540 (1997).

[44] S. Weinberg, *Gravitation and Cosmology* (Wiley, New York, 1972).
[45] G. Baym, C. Pethick, and P. Sutherland, Astrophys. J. **170**, 299 (1971).
[46] J. M. Lattimer, M. Prakash, D. Masak, and A. Yahil, Astrophys. J. **355**, 241 (1990).
[47] J. M. Lattimer and M. Prakash, Astrophys. J. **550**, 426 (2001).
[48] J. M. Lattimer and M. Prakash, Science **304**, 536 (2004).
[49] J. Schaffner and I. N. Mishustin, Phys. Rev. C **53**, 1416 (1996).
[50] H. Shen, Phys. Rev. C **65**, 035802 (2002).
[51] M. Bejger, T. Bulik, and P. Haensel, Mon. Not. R. Astron. Soc. **364**, 635 (2005).
[52] C. O. Heinke, G. B. Rybicki, R. Narayan, and J. E. Grindlay, Astrophys. J. **644**, 1090 (2006).
[53] F. Ozel, Nature (London) **441**, 1115 (2006).
[54] A. R. Villarreal and T. E. Strohmayer, Astrophys. J. **614**, L121 (2004).
[55] Y. Sugahara and H. Toki, Prog. Theor. Phys. **92**, 803 (1994).
[56] V. Greco, F. Matera, M. Colonna, M. Di Toro, and G. Fabbri, Phys. Rev. C **63**, 035202 (2001).
[57] P. K. Panda, J. da Providência, and C. Providência, Phys. Rev. C **73**, 035805 (2006).
[58] S. L. Shapiro and S. A. Teukolsky, *Black Holes, White Dwarfs, and Neutron Stars* (Wiley, New York, 1983).
[59] N. Stergioulas and J. L. Friedman, Astrophys. J. **444**, 306 (1995).
[60] M. Bejger, P. Haensel, and J. Zdunik, Astron. Astrophys. **464**, L49 (2007).
[61] P. Danielewicz, R. Lacey, and G. Lynch, Science **298**, 1592 (2002).